NANO EXPRESS

Influence of Anodic Conditions on Self-ordered Growth of Highly Aligned Titanium Oxide Nanopores

V. Vega · Victor M. Prida · M. Hernández-Vélez ·
E. Manova · P. Aranda · E. Ruiz-Hitzky ·
Manuel Vázquez

Abstract Self-aligned nanoporous TiO_2 templates synthesized via dc current electrochemical anodization have been carefully analyzed. The influence of environmental temperature during the anodization, ranging from 2 °C to ambient, on the structure and morphology of the nanoporous oxide formation has been investigated, as well as that of the HF electrolyte chemical composition, its concentration and their mixtures with other acids employed for the anodization. Arrays of self-assembled titania nanopores with inner pores diameter ranging between 50 and 100 nm, wall thickness around 20–60 nm and 300 nm in length, are grown in amorphous phase, vertical to the Ti substrate, parallel aligned to each other and uniformly disordering distributed over all the sample surface. Additional remarks about the photoluminiscence properties of the titania nanoporous templates and the magnetic behavior of the Ni filled nanoporous semiconductor Ti oxide template are also included.

Keywords Titanium oxides · Nanoporous materials · Electrochemical anodization

V. Vega · V. M. Prida (✉)
Depto. Física, Universidad Oviedo, Calvo Sotelo s/n, Oviedo
33007, Spain
e-mail: vmpp@uniovi.es

M. Hernández-Vélez · E. Manova · P. Aranda ·
E. Ruiz-Hitzky · M. Vázquez
Instituto Ciencia Materiales Madrid (CSIC), Cantoblanco,
Madrid 28049, Spain

M. Hernández-Vélez
Depto. Física Aplicada C-XII, UAM, Cantoblanco, Madrid
28049, Spain

Introduction

Nanodimensional structures including nanotubes, nanowires and nanoporous architectured materials based on semiconducting metal oxides have become of fundamental interest to the development of functional nanomaterials, nanodevices and nano-systems [1]. Recently, the synthesis of nanostructured functional oxides based on transition metals, with controlled structure and morphology, has attracted a huge interest due to their potential applications in a broad research fields such as Nanoelectronic, Spintronic, Fuel Cells, Nano-biotechnological or Magneto-optoelectronic devices. These new materials have shown a broad range of novel and enhanced mechanical, optical, magnetic and electronic properties respect to those showed by their bulk analogues [2–5]. Actually, great efforts are made in order to obtain self-assembled nanostructures based on TiO_2 nanoporous membranes prepared by sol–gel coating [6], nano-imprint [7], or electrochemical processes [8]. The search is focused to low cost and efficient fabrication techniques of nanostructured transition metal oxides with high quality nanoporous structures over large surface areas and an accurate pore size control together with long range ordering to enhance the efficiencies of devices based on nanoporous titania (TiO_2) templates [9]. The principal advantages for using pure titanium and its alloys are, among others, their high corrosion and good oxidation resistances, low density, high yield strength in a wide temperature range and excellent biocompatibility, which becomes this metal in an outstanding candidate for its application in a wide scientific and technological areas, as e.g. in biocompatible biomaterials, semiconductor memory alloy devices, diluted magnetic semiconductors and materials for micro-optoelectronic applications, transparent oxides semiconductors and gas/humidity or conductivity

sensors [10–15]. Otherwise, some of these properties adequately combined with the large band gap semiconductor properties, a high photo-catalytic activity and an excellent biocompatibility exhibited by the TiO$_2$ converts it in a very promising material for applications in many scientific and technological areas, e.g., biocompatible biomaterials for bone implants [16] or transcutaneous hydrogen sensors [17], semiconductor memory alloy devices [18], materials for optoelectronic applications [19], gas/humidity or conductivity sensors [11], among others.

The low cost-effective obtention of nanoarchitectured semiconducting metal oxides with high quality nanoporous structures over large surface areas and with precise control of pore size and periodic ordered degree distribution, still remains as an open task. It is undoubted that the control of all these requirements must be fulfilled at the same time in order to optimize the efficiency of the devices based on the titania (TiO$_2$) nanopore arrays [10, 12]. The existence of two unique structural features in these nanostructured semiconducting oxide such as, mixed cation valences and an adjustable oxygen deficiency put the basis for creating and tuning many novel material properties, as well which, allow to use them in the design of sensors and functional devices with superior performance [11–19].

In this work we report about the temperature parameter and acidic electrolyte media influence on the self-aligned and randomly disordered growth of titania nanopore arrays, synthesized by using a very simple and recently reported electrochemical anodization technique [8]. We have focused our attention on the pore size distribution of titania nanopore arrays and the formation of stable and larger wall thicknesses on the wide nanoporous surface obtained, which greatly depend on the experimental anodic parameters. We have extensively studied the titania nanopore arrays growth with varying the anodization temperatures, under different ambient conditions and also, varying the chemical concentrations of the acid electrolytic media. Recently, we have also reported about the magnetic behavior of ferromagnetic nanowires grown inside semiconducting titania nanopores array by electrodeposition technique, using them as templates [20]. Finally, some remarks about the main applications based on these nanoporous semiconductor oxide nanostructures are briefly discussed.

Experimental Details

Small pieces of high purity Titanium foils (99.95+%, Goodfellow) with 2.25 mm^2 surface area and 25 μm of thickness were employed as starting metal to obtain self-aligned TiO$_2$ nanopores through an unique anodization process [8]. Prior to the anodization, the Titanium sheets

were smooth out mechanically up to mirror polishing, and afterwards the polished titanium foils were ultrasonically degreased and cleaned in isopropanol, acetone and ethanol, and finally they were rinsed out with abundant deionised water (18.2 MΩ).

The single anodization processes to obtain self-aligned nanoporous titanium dioxide were always carried out potentiostatically in a homemade designed electrochemical cell by using a direct current (dc) source, that was kept to a constant voltage value of 20 V during the whole processes at several temperatures ranging from 2 °C to ambient and different times from 20 min up to several hours [21]. A Pt grid of large surface area was used as a cathodic counter electrode, as it can be seen in Fig. 1, where a scheme of the experimental setup employed for the single anodization process of the Ti foil is shown in the Fig. 1; up we show a schematic diagram of the anodization cell, where the Ti foil makes as the cathodic electrode and a Pt grid makes as the anode, being the electrolyte a mixture of aqueous solution of fluoride acids; down, it is drawn a picture of the synthesized titania nanoporous arrays obtained after the anodization process, where an enlargement of a single titanium dioxide nanopore is also depicted. Anodic experiments were also made at different temperatures varying from 2 °C up to ambient temperature (20 °C). Hydrofluoric acidic (0.15–0.5 wt.%) aqueous solutions and its mixtures with H$_2$SO$_4$ (1 M) were used as electrolytes, which were mechanically stirred during the process by using an electric blender. Solutions pH values of the electrolytes were varied from 3.2 to 2.2.
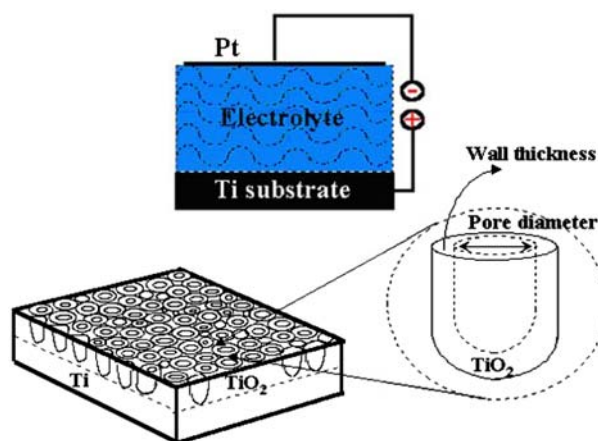

Fig. 1 Scheme of the single anodization process for the synthesis of titania nanopores arrays: up, it is shown a schematic diagram of the homemade electrolytic cell employed during the anodization processes, down it is depicted the titania nanopore arrays grown on the Ti layer synthesized after the single anodization process. An enlargement of a single titanium dioxide nanopore is also represented in the magnification

Titania nanoporous array microstructures were studied by using an X'pert-APD Philips X-ray diffractometer. The morphology and atomic chemical microanalysis by energy dispersive X-ray spectroscopy (EDX), of the so-obtained anodized nanoporous titanium dioxide layers, were characterized with HITACHI S-800 and JEOL, JSM-6100, Scanning Electron Microscopes (SEM). Atomic Force Microscopy (AFM) in dynamic mode was also used for surface characterization.

The depth profiling analysis for the titania nanopores arrays were carried out by means of a radiofrequency Glow Discharge Optical Emission Spectroscopy (rf-GD-OES) technique operated with Ar by using a commercial JY 5000 RF instrument working at 13.56 MHz [22]. The samples taken as cathodes were placed in a holder and submitted to a previous vacuum during 5 min. The arrays of the randomly disordered and self-aligned titania nanopores were sputtered in Argon atmosphere at 600 Pa and applied power of 40 W. Data were collected from a nanoporous array circular area of 4 mm in diameter. The wavelengths of spectral emission lines employed for detecting sputtered specimens of Ti, C, O, S, and Ar were 365, 156, 130, 181, and 404 nm, respectively. The sputtering rate and penetration depths were obtained from calibration by direct profilometer measurements, (Perth-o-meter S5P, Mahr Perthen) [23].

Afterwards, the nanoporous anodic TiO_2 templates were also filled with Ni by means of an electrodeposition technique, by using an alternating pulse method reported elsewhere [24]. The metallic Ni nanowire arrays were electrochemical grown into the titania nanopores employing the Watts-bath electrolyte [21], where the temperature and pH values where kept between 35–40 °C and 4.5, respectively and the electrodeposition time was ranged from 20 min to 1 h.

Magnetic characterization of the Ni electrodeposited samples were carried out through the hysteresis loops measurements in parallel and perpendicular configurations to the Ni nanowires axis at room temperature by using a VSM magnetometer in the range of the applied magnetic field up to 10^4 Oe (1 Tesla). The sample was mounted in the slot of a plastic holder which, likewise, was placed into the magnetic field of the magnetometer. Turning the sample holder allowed hysteresis loop measurements to be performed for the applied magnetic field aligned both along, and transverse to the long axis of the Ni nanowires.

Structure and Morphology of the Anodic Titanium Oxide Nanopores Array

The metal oxides anodic growth depends on the rate of ion-transfer reactions at the metal/oxide/electrolyte interface,

as well as other solid state properties of the oxide film such as its electronic and ionic conductivity, potential distribution and surface structure [25]. Figure 2a and b show the voltage and current transients (V-t, I-t curves) recorded during Ti anodization process, for the case of employing different electrolytes and temperatures during the anodic process. It can be observed in the Fig. 2a, that in the first few seconds of the anodic process a current exponential decay occurs; and later on, the current starts slowly to increase up to a quasi-steady state, which is reached along the first minutes of the anodization process. The strong current exponential decay occurred during the first stage corresponds to titanium oxide barrier growth. Since the ionic current density depends exponentially on the field strength across the oxide an increase of oxide thickness causes a decrease of the field strength and therefore, an exponential decrease of the anodic current takes place [25].

Due to the solubility of the titanium oxide in HF-containing electrolytes the current starts to increase in the next stage leading to the random growth of titanium oxide
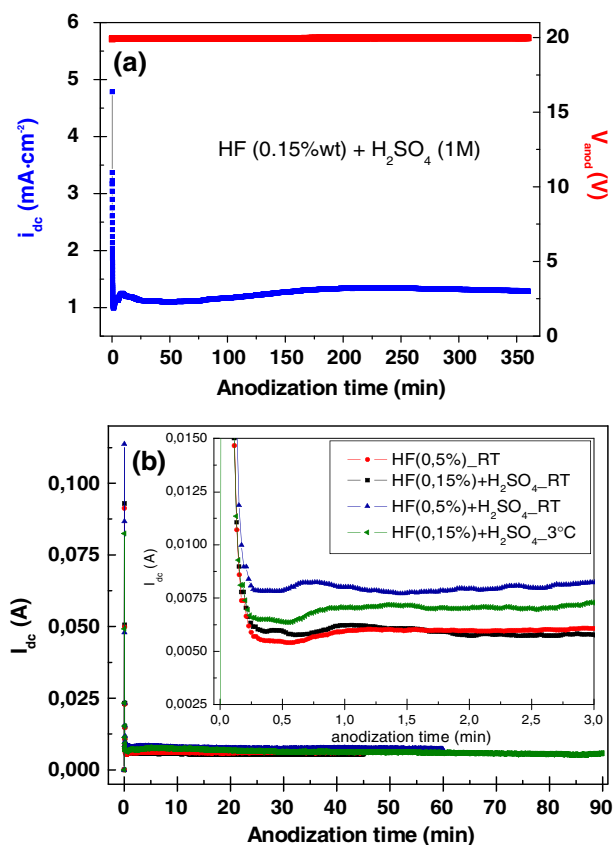

Fig. 2 (**a**) Voltage and current density transients corresponding to an anodic process during the self-assembling formation of titania nanopores in a mixture of HF + H_2SO_4 electrolytes at RT; (**b**) I-t current transients recorded at constant voltage of 20 V_{dc} during the anodizing processes of Ti films at different temperatures, times and electrolyte solutions

nanopores. The presence of fluoride ions in the electrolyte has been previously demonstrated to be necessary for the occurrence of the titania porous structure growth [8, 11, 26, 27]. Along the last stage, a more stable and regular self-aligned titania nanopores growth is established and therefore the current starts slowly to decrease again. Periodical fluctuations exhibited by the current remaining after the reached quasi-steady-state can be also appreciated during the current transients. Such strong current oscillations occurred during titanium anodization have been ascribed to a passivation and depassivation reactions related to the TiO_2 porous layer formation and oxide dissolution which are competing during the self-aligned titania nanopores growth [26].

The Fig. 2b shows the current transients (I_{dc}-t) recorded during Ti anodizations at constant voltage of 20 V_{dc} in different mixtures of aqueous acidic solutions of HF and H_2SO_4 electrolytes, temperatures and times of the anodic process. It can be seen that for the different curves reported, similar processes take place to before described in Fig. 2a, briefly they are: during the first few seconds of the anodization a drastic current exponential drop due to the formation of compact oxide film which increases the resistance reducing the current densities, followed by a next stage where the current intensity starts to increase due to the solubility of the Ti oxide in acidic HF-containing solutions and nanopores begin to grow randomly. This is followed by a more stable and regular competition between the self-aligned titania nanopores growth and therefore, the current starts slowly to decrease again. The inset of Fig. 2b shows the typical current intensity fluctuations which are closely related to the growth and dissolutions of the oxide films, ascribed to a passivation and depassivation reactions related to the nanoporous TiO_2 formation and oxide dissolution. In fluoride-containing electrolytes, the anodization of Ti is accompanied with the chemical dissolution of Ti oxide due to the formation of TiF_6^{2-} [28]. This dynamic oxide formation/dissolution equilibrium established during large periods of the anodization process, controls the time scale of the porosity developed, self-ordering effects and the thickness of the oxide layer. This mechanism of oxide growth is typical for the self-inhibited semiconducting oxides formation, where a potential drop is located in the space charge layer near the oxide surface during the oxide film thickness growth.

The titanium anodized samples in HF acidic solutions yields a regular self-aligned and randomly disordered grown nanopores array over large areas of the sample substrate, over more than hundred of microns, as it can be seen from the SEM top-view images shown in Fig. 3a–c for both cases: a sample anodized at 20 V during 90 minutes in HF (0.5 wt.%) acid at room temperature Fig. 3a, a sample anodized at 20 V during 18 h in a mixture of HF (0.15 wt.%) plus H_2SO_4 (1 M) at RT in Fig. 3b,

and after following the same process than in Fig. 3b) but at 4 °C is shown in Fig. 3c, respectively. The corresponding histograms with the pore diameter distribution of the so-formed TiO_2 nanopores are also shown in each case. The self-aligned tubular structure exhibited in the SEM image shown in Fig. 3a, has an average inner pore diameter of 65 ± 10 nm and a nearly uniform wall thickness above 25 ± 10 nm, similar to the values reported elsewhere [8, 28]. Therefore, the resulting average outer diameter of the titania nanopores ranges between 90–110 nm. Meanwhile, for the case of the sample anodized in a mixture of HF 0.15 wt.% and H_2SO_4 (1 M) acidic electrolytes at RT, shown in Fig. 3b), the resulting average inner pore diameter is approximately about 75 ± 10 nm and the wall thickness of the pores about 20 ± 10 nm, as it is clearly seen in the corresponding histogram. Otherwise, for the sample anodized in the same mixture than before mentioned electrolyte but employing the low temperature range of 4 °C, the nanopore diameters reach about 55 and 40 nm of wall thickness. Therefore, the fluoride concentration do not influences so much the titania nanopores diameter but it appears that temperature of anodic process so does it [29].

The different anodizing conditions employed lead to different stages of the surface structures of nanoporous titania, where highly self-aligned nanopores arrays are formed at low anodic potentials as a resulting of the electrochemical etching, as it can be seen in the HR-SEM top-view images of the Fig. 4a–d), corresponding to the surface structures obtained for the anodized Ti samples under different ambient conditions. In Fig. 4a) we show the nanoporous titanium oxide formed onto the film substrate in the first stages of the anodization process. Fig. 4b) shows the formation of a spongelike randomly porous structure at the low temperature of 2 °C in HF electrolyte. Low temperature anodization appears to inhibit the nanotubular structure formation. Meanwhile, the straight nanopores obtained at RT anodic processes have a pore size ranging between 60 to 100 nm and 25–40 nm wall thickness, as it can be observed in Fig. 4c and d, where the anodic electrolytes employed were a HF (0.5 wt.%) aqueous solution at 20 V and RT, and a H_2SO_4 solution mixed with HF (0.15 wt.%) acid at 20 V, during 1.5 and 6 h at RT, respectively [29].

Energy dispersive X-ray spectroscopy (EDX) shown in Fig. 5, in the SEM, was used to confirm the atomic compositional analysis of the titania nanopores, which exhibit an atomic concentration of approximately 58–60% titanium and 36–42% oxygen for the nanoporous layer, appearing evident that the nanopores array composition consists of TiO_2.

The electrolyte composition and applied anodic potential primarily determine the oxide structure resulting from the anodic process. The analysis of the X-ray pattern

Fig. 3 Top-view SEM images for the self-organized nanoporous titanium oxide templates obtained by anodization processes: (**a**) self-aligned and randomly disordered nanoporous titania template after being submitted a single anodic process in hydrofluoric acid solution for 90 min at RT; (**b**) in a mixture of hydrofluoric plus sulphuric acid solution during 18 h at RT; and (**c**) similar treatment to (**b**) at 4 °C, respectively. Their corresponding histograms with the pore diameter distribution of the so-formed TiO_2 nanopores are also shown
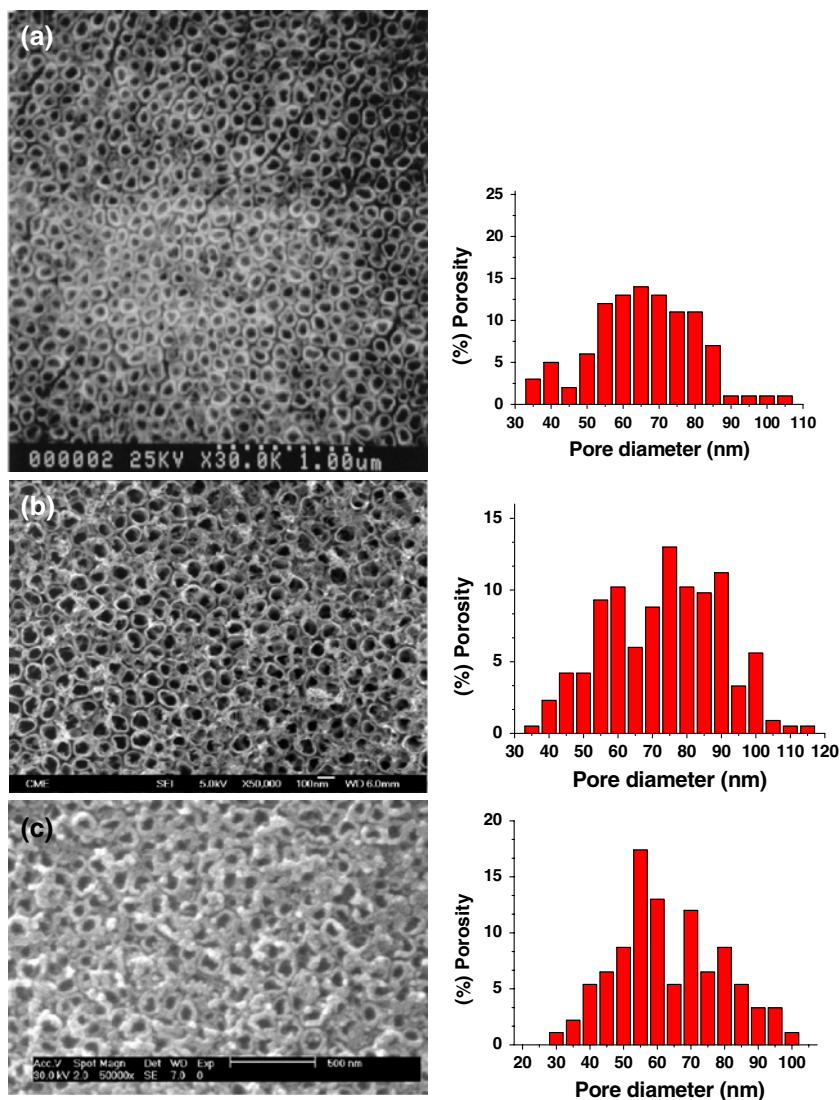
diffraction data shown in the Fig. 6 indicates that the only observed reflections correspond to Ti substrate, while neither rutile not anatase Ti crystalline phases are present. That allows us to infer the amorphous character of the anodic grown Ti oxide. This result agrees well with the reported structure for the obtained self-inhibiting oxide films that have been synthesized after similar anodization process at low potentiostatic voltages, typically below 20 V [11, 25].

A rf-GDOES qualitative depth profile of a self-aligned titania nanopores array is shown in Fig. 7, for the sample anodized in HF mixed with H_2SO_4 acidic electrolytes. The direct analysis performed with this technique reveals its ability to control the quality and testing the composition of the nanoporous structure along the depth profile of the samples. As it can be seen in the Fig. 7, the signal intensities of carbon and oxygen remain relatively steady along the first hundred of nm in depth. Since the signal intensity

for the titanium increases sharply up to its maximum Ti substrate signal, also decreasing at the same time the corresponding one for the oxygen, it allows to be well defined the oxide/substrate interface. Signal intensities from S are due to the SO_4^{2-} anions present during the anodic process, and Ar traces are provided for the trapped gas during plasma ionization, which are also clearly revealed. Assuming a constant rate of Ar sputtering of 4 μm/min. across throughout the thickness film, the estimated length for the grown titania nanopores results about 300 nm. For these self-inhibiting systems the total oxide film thickness increases almost linearly with the electrode potential, since the rate determining step is the ionic migration within the oxide. This would correspond to a Ti oxide layer growth rate about 15 nm/V, formed far below the dielectric breakdown voltage, typically above 100 V for these materials [20, 23]. The inset shows a SEM image corresponding to a slightly tilted nanoporous titania sample,

Fig. 4 Top-view HR-SEM images of the surface structure obtained from anodic Titanium films after the following conditions: (**a**) anodized in HF at RT during 20 s; (**b**) HF at 2 °C during 2 h; (**c**) HF at RT during 1.5 h; and (**d**) HF + H_2SO_4 at RT during 6 h
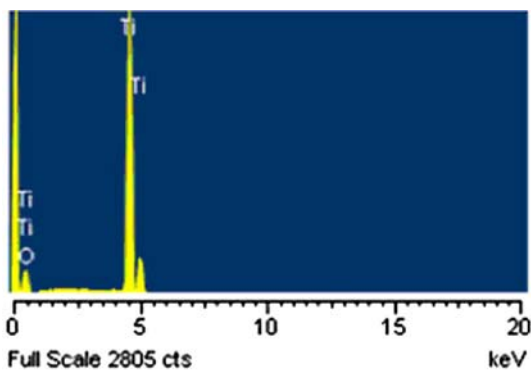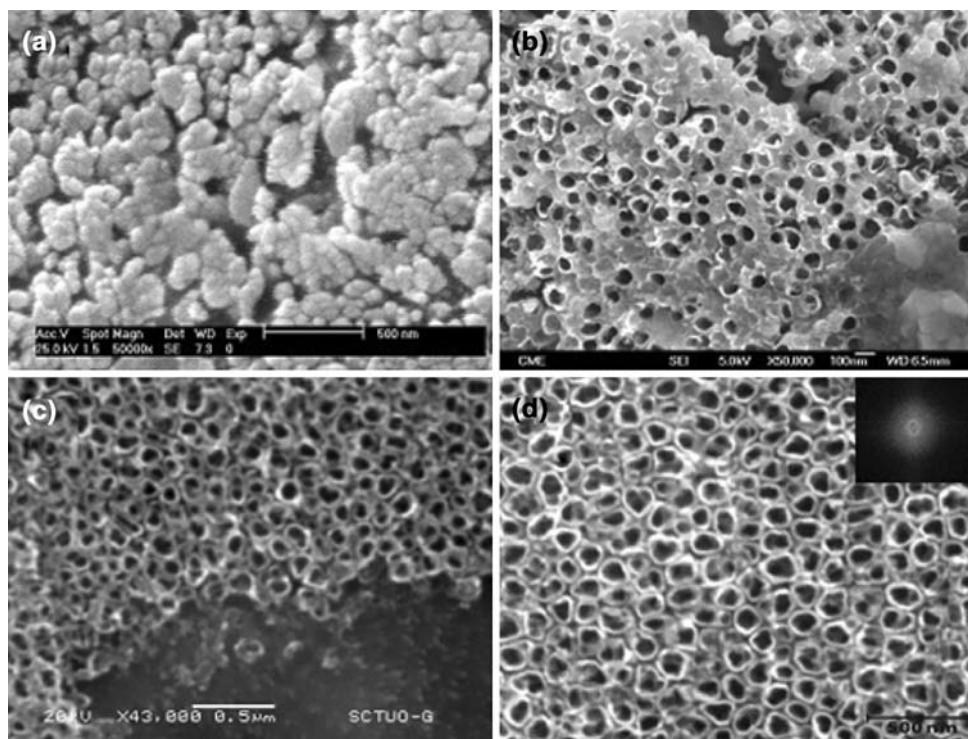

Fig. 5 EDX spectrum showing the chemical compositional traces for the self-assembled TiO_2 nanopores array

Fig. 6 X-ray diffraction patterns corresponding to: (**a**) as-received Ti foil; (**b**) Ti film anodized in HF (0.15 wt.%); (**c**) anodized in HF (0.5 wt.%) at RT; (**d**) anodized in HF (0.15 wt.%) at 2 °C; and (**e**) Ti film anodized in HF (0.15 wt.%) + H_2SO_4 (1 M) at RT. In all the cases the samples were anodized at 20 V_{dc}

where it can be clearly seen the highly self-aligned nano-columns formed by the TiO_2 nanopores grown.

Self-assembled TiO_2 Nanopores Arrays as Templates for Applications

The semiconducting and photoelectrochemical properties exhibited by the nanoporous amorphous structure of the anodic TiO_2 oxide are very promising for their applications in the designing of photo-catalyst and solar cells based devices [10, 30–32], so as in the construction of hydrogen storage and sensors devices also [33]. The Fig. 8a and b
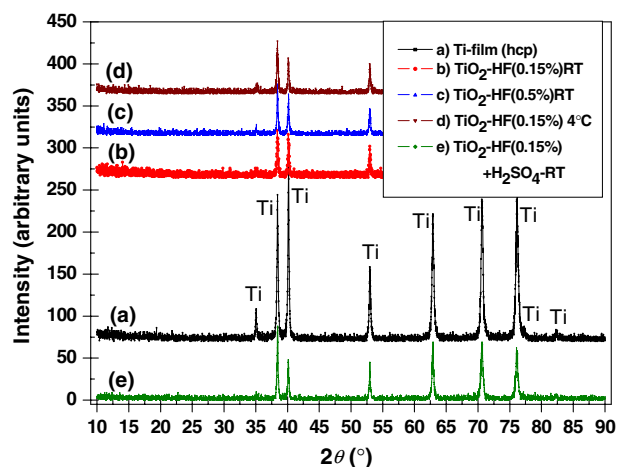
show the photoluminescence (PL) and Raman spectra corresponding to a nanoporous sample formed by self-aligned TiO_2 nanopores, respectively. In the PL spectrum of a self-aligned titania nanopores array shown in the Fig. 8a, a broad emission band of around 0.8 eV in the wavelength range between 580–780 nm can be clearly observed. Otherwise, the Raman spectrum of a nanoporous titania template synthesized after following the anodic conditions above mentioned, shown in the Fig. 8b, the
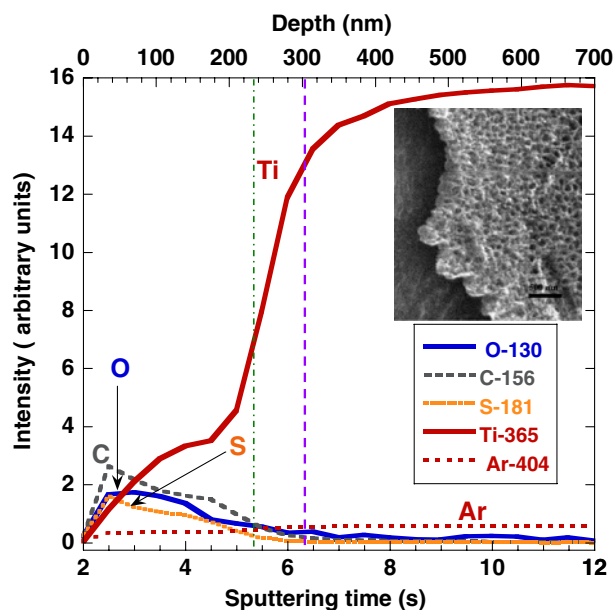
Fig. 7 Qualitative rf-GDOES depth profile spectrum of an array of nanoporous titania template. Relevant wavelengths (nm) of the spectral emission lines are listed. The inset shows the SEM image of a tilted TiO_2 nanopores template

spectrum has been collected at tree different wavelength ranges, for a data storage time of 240 s. Si was used as reference spectrum, and the appearance of spurious signals observed in the nanoporous TiO_2 membrane spectrum is actually under analysis. It can be derived from the experimental results that the semiconducting optimal conditions exhibited by the nanoporous structure of the self-assembled titania nanotube templates are a consequence of the impurities and defects present in the titania nanotube walls, which exhibit different densities of donors concentrations from the bottom of the nanopores to the surface along the nanotube walls. The semiconductor behavior of these nanotubular oxides can be well explained considering a high concentration of electronic defects in the wall of oxide nanopores, which are in electronic equilibrium with the underlying compact oxide at the bottom. In this structure, the surface chemistry of tubes introduces considerable changes in the semiconductor behavior of the underlying oxide, which in turn is manifested in surface related effects, giving rise to modifications of the redox reactions and a shift of the flat band potential respect to the base oxide, and trapping of photoelectrons [30–33].

Other kind of interesting applications for the nanoporous titania templates are based on doping semiconductor titanium oxide with magnetic materials for diluted magnetic semiconductors and/or spintronics [13, 34].

The synthesis of magnetic metallic nanowires based on self-assembled templates is of increasing interest for fundamental magnetic materials research, because of the
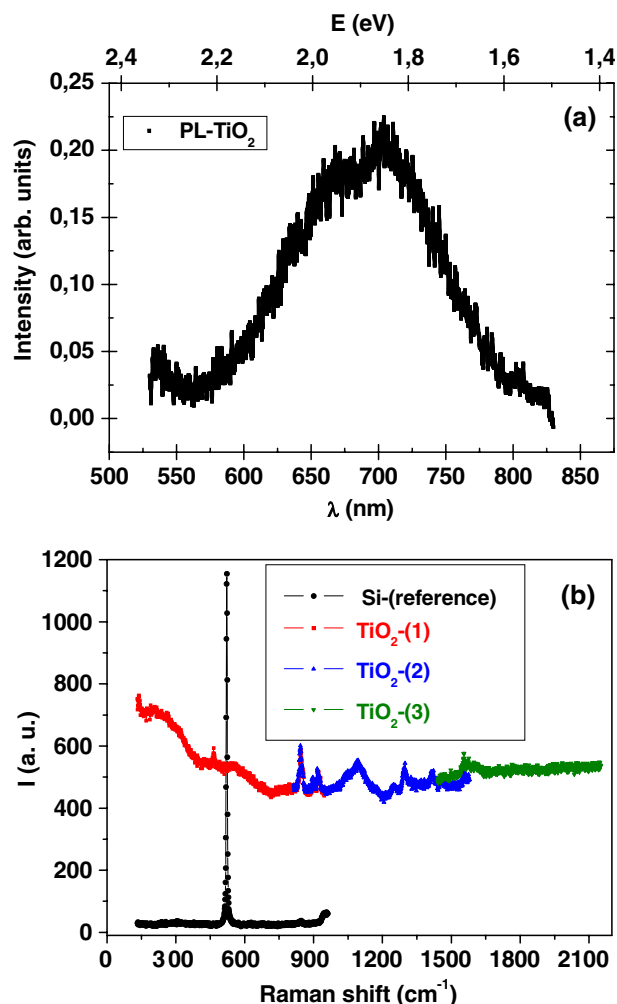

Fig. 8 (**a**) Photoluminescence spectrum of a self-aligned titania nanopores array; (**b**) Raman spectra of a nanoporous titania membrane anodized following the conditions above mentioned, Si is used as reference spectrum

relation of the geometric dimensions of a nanosized metallic wire and its magnetic behavior [35]. Composites based in self-ordered membranes filled with arrays of magnetic nanowires are ideal systems to study the anisotropic magnetic nature of the metallic wires. The shape anisotropy of an individual wire can cause two possible stable magnetic moment orientations, well parallel or perpendicular to the wire axis, as it can be derived from hysteresis loop measurements. Ferromagnetic Ni metallic nanowires were grown inside the self-aligned randomly disordered nanoporous titania templates by using a modulated pulsed electrodeposition method [24], for a time process ranging from 15 min up to 1 h [21], as it can be shown in the Fig. 9. In the Fig. 10, it can be appreciated the room temperature VSM hysteresis loops for both possible magnetic configurations, that means, when the magnetic field is applied parallel to the Ni nanowires axis ($M_{parallel}$),
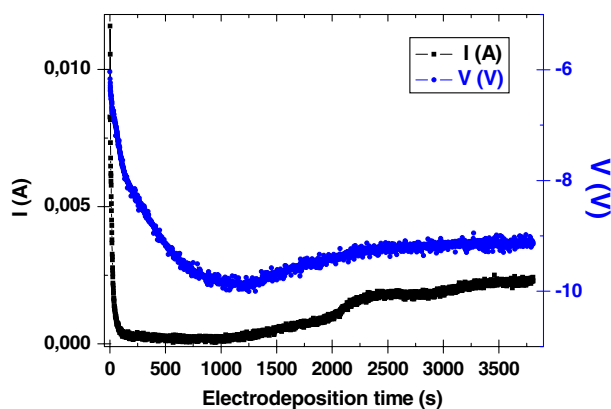
Fig. 9 Current and voltage transients during the alternating pulsed electrodeposition process of Ni into a nanoporous titania template
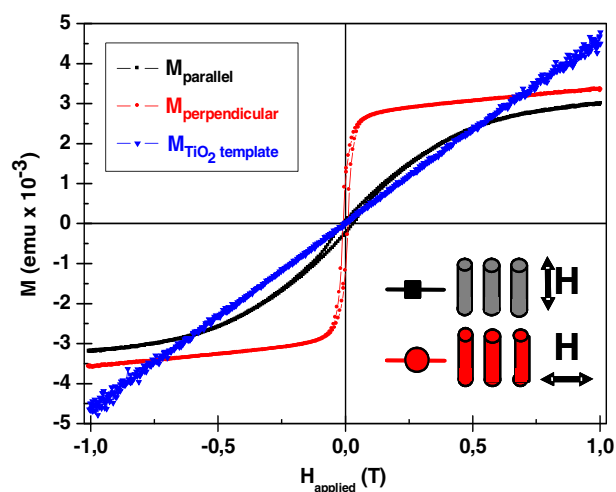

Fig. 10 VSM hysteresis loops of arrays of Ni nanowires electrochemical embedded in self-aligned nanoporous TiO$_2$ template, with applied magnetic field parallel (■) and perpendicular (•) to the nanowire axis, the paramagnetic behaviour of the Ti substrate is also shown

(therefore also along titania nanopores), and another case when the applied magnetic field is perpendicular to the Ni nanowires axis ($M_{perpendicular}$). In both cases the VSM hysteresis loops were obtained for an array of Ni nanowires prepared by electroplating during 60 minutes filling into the self-aligned nanopores of a titania template having an average inner pore diameter of 100 nm, 40–60 nm wall thickness and around 300 nm in depth. The $M_{parallel}$ hysteresis loop corresponds to a hard magnetization axis of the Ni nanowires array showing a coercive field, H$_C$~199 Oe, meanwhile the $M_{perpendicular}$ hysteresis loop is typical from an easy magnetization axis, with a coercive field about 98 Oe.

It has been previously established that the pure TiO$_2$ do not shows any ferromagnetic behavior [10, 21], therefore it appears evident that the peculiar ferromagnetic long-range

order exhibited is due to the Ni electrodeposition filled titania nanopores. A paramagnetic contribution from the Ti substrate to the magnetic signal of the nanowires can also be clearly detected [21]. Since the Ni nanowires were synthesized employing commercial electrolytes, the co-deposition of impurities from the electrolytes could cause the magnetization of the Ni nanowires array to be smaller than that of the pure metals.

The magnetic behavior exhibited by the peculiar shape of the hysteresis loops of the arrays of Ni nanowires embedded into the self-aligned and randomly disordered amorphous TiO$_2$ nanopores, is very similar to the case of Ni nanowire arrays with large diameter nanowires and quite high aspect ratio (length/diameter) about 2.3–2.4, as reported from others [21]. The coercivity and remanence given values would correspond to a vortex-state nanowire, where the magnetization adopts a helical structure beginning to tilt in the circumferential direction, starting at the ends of the wire, giving rise to a circumferential magnetization at the wire's perimeter while the magnetization at the center of the wire remains oriented along its axis. The vortex-type remanent magnetization distribution in these flat nanowires can be created due to the strong magnetic interactions between the larger-diameter particles, helped by the minor role that plays the weak magnetocrystalline anisotropy of the policrystalline Ni at room temperature [35]. In fact, reducing the wires height to diameter ratio favors the $M_{perpendicular}$ magnetized state. Besides that, when the inter-wires spacing makes small as compared to the nanowires diameter, the magnetostatic interactions between the coupled nanowires can be so strong as to make the $M_{perpendicular}$ direction as the easy magnetization axis. Additionally, the $M_{perpendicular}$ coercivity of these Ni nanowires is low due to the vortex magnetic configuration can cause partial flux closure which reduces it, since it results relatively easy to move a vortex or domain wall through the particles [21]. Magnetic nanowires exhibiting vortex domain state have typical switching field values around hundreds of Oe, as a result of differences in the shapes, heights, microstructures, roughness or inhomogeneities of the particles, that can act as pinning centers of the magnetization as it rotates in plane. Moreover, vortex states in the nanowires formed by short, but high enough aspect ratio, and closely spaced interacting wires can give rise to a larger saturation field in the $M_{parallel}$ direction and low remanence, which is consistent with strong interactions. These novelty nanocomposites, based on ferromagnetic nanowires embedded in anodic nanoporous semiconducting TiO$_2$ templates, can become in a promising candidates for many applications in a broad range of scientific and technological areas, such as functionalized arrays for magnetic sensing, ultrahigh density magnetic storage media or spin-based electronic devices.

References

1. G.Q. Lu, X.S. Zhao, in *Nanoporous Materials: Science and Engineering*, Vol. 4, ed. by T.K. Wei (Series on Chemical Engineering, Imperial College Press, London, 2004)
2. C.R. Martin, Science **266**, 1961 (1994)
3. J.R. Heath, Science **270**, 1315 (1995)
4. J.M. García, A. Asenjo, J. Velázquez, D. García, M. Vázquez, P. Aranda, E. Ruiz-Hitzky, J. Appl. Phys. **85**, 5480 (1999); M. Vázquez, K. Pirota, M. Hernandez-Velez, V.M. Prida, D. Navas, R. Sanz, F. Batallan, J. Appl. Phys. **95**, 6642 (2004)
5. C.M. Lieber, Nano Lett. **2**, 81 (2002)
6. P. Hoyer, Langmuir **12**, 1411 (1996)
7. H. Masuda, K. Nishio, N. Baba, Jpn. J. Appl. Phys. **31**, L1775 (1992)
8. D. Wong, C.A. Grimes, O.K. Varghese, W. Hu, R.S. Singh, Z. Chen, E.C. Dickey, J. Mater. Res. **16**, 3331 (2001)
9. M. Vazquez, M. Hernandez-Velez, A. Asenjo, D. Navas, K. Pirota, V. Prida, O. Sanchez, J.L. Baldonedo, Phys. B **384**, 36 (2006)
10. U. Diebold, Surf. Sci. Rep. **48**, 53 (2003)
11. O.K. Varghese, D. Gong, M. Paulose, K.G. Ong, E.C. Dickey, C.A. Grimes, Adv. Mater. **15**, 624 (2003); G.K. Mor, O.K. Varghese, M.Paulose, C.A. Grimes, Sensor Lett. **1**, 42 (2003)
12. Z.L. Wang, Adv. Mater. **15**, 432 (2003)
13. J.S. Kulkarni, O. Kazakova, J.D. Holmes, Appl. Phys. A **85**, 277 (2006)
14. H. Osono, Thin Solid Films **515**, 6000 (2007)
15. H. Wang, C.T. Yip, K.Y. Chenng, A.B. Djurisic, M.H. Xie, Y.H. Lenng, W.K. Chan, Appl. Phys. Lett. **89**, 023508 (2006); Q. Zhou, Y. Ding, J. Xiao, G. Liu, X. Guo, J. Chromatogr. A **1147**, 10 (2007)
16. D. Velten, V. Biehl, F. Aubertin, B. Valeske, W. Possart, J. Breme, J. Biomed. Mater. Res. **59**, 18 (2002); H.-C. Cheng, S.-Y. Lee, C.-C. Chen, Y.-C. Shyng, K.-L. Ou, Appl. Phys. Lett. **89**, 173902 (2006)
17. O.K. Varghese, X. Yang, J. Kendig, M. Paulose, K. Zeng, C. Palmer, K.G. Ong, C.A. Grimes, Sensor Lett. **4**, 120 (2006)
18. T. Ohtsuka, T. Otsuki, Corr. Sci. **40**, 951 (1998)
19. R. Vogel, P. Meredith, I. Kartini, M. Harvey, J.D. Riches, A. Bishop, N. Heckenberg, M. Trau, H. Rubinsztein-Dunlop, ChemPhysChem. **4**, 595 (2003)
20. V.M. Prida, M. Hernandez-Velez, M. Cervera, K. Pirota, R. Sanz, D. Navas, A. Asenjo, P. Aranda, E. Ruiz-Hitzky, F. Batallan, M. Vazquez, B. Hernando, A. Menendez, N. Bordel, R. Pereiro, J. Magn. Magn. Mater. **294**, e69 (2005)
21. V.M. Prida, M. Hernández-Vélez, K.R. Pirota, A. Menéndez, M. Vázquez, Nanotechnology **16**, 2696 (2005)
22. J. Pisonero, B. Fernandez, R. Pereiro, N. Bordel, A. Sanz-Medel, Trends Analyt. Chem. **25**, 11 (2006)
23. V.M. Prida, D. Navas, K.R. Pirota, M. Hernández-Vélez, A. Menéndez, N. Bordel, R. Pereiro, A. Sanz-Medel, B. Hernando, M. Vázquez, Phys. Stat. Sol. A **203**, 1241 (2006)
24. K.R. Pirota, D. Navas, M. Hernandez-Velez, K. Nielsch, M. Vazquez, J. Alloys Compounds **369**, 18 (2004)
25. J.W. Schultze, M.M. Lohrengel, D. Ross, Electrochim. Acta **28**, 973 (1983)
26. V. Zwilling, E. Darque-Ceretti, A. Boutry-Forveille, D. David, M.Y. Perrin, M. Aucouturier, Surf. Interface Anal. **27**, 629 (1999); R. Beranek, H. Hildebrand, P. Schmuki, Electrochem. Solid State Lett. **6**, B12 (2003)
27. J. Zhao, X. Wang, T. Sun, L. Li, Nanotechnology **16**, 2450 (2005)
28. R. Beranek, H. Tsuchiya, T. Sugishima, J.M. Macak, L. Traveira, S. Fujimoto, H. Kisch, P. Schmuki, Appl. Phys. Lett. **87**, 243114 (2005)
29. Q. Cai, M. Paulose, O.K. Varghese, C.A. Grimes, J. Mater. Res. **20**, 230 (2005)
30. A.G. Muñoz, Electrochim. Acta **52**, 4167 (2007)
31. E. Fortunato, D. Ginley, H. Hosono, D.C. Paine, MRS Bull. **32**, 242 (2007)
32. S.P. Albu, A. Ghicov, J.M. Macak, R. Hahn, P. Schmuki, Nano Lett. **7**, 1286 (2007)
33. G.K. Mor, M.A. Carvalho, O.K. Varghese, M.V. Pishko, C.A. Grimes, J. Mater. Res. **19**, 628 (2004)
34. X. Huang, G.J. Ackland, K.M. Rabe, Nat. Mater. **2**, 307 (2003)
35. V.M. Prida, K.R. Pirota, D. Navas, A. Asenjo, M. Hernández-Vélez, M. Vázquez, J. Nanosci. Nanotechnol. **7**, 272 (2007)